Numerical Heat Transfer, Part A, 54: 665–685, 2008

ISSN: 1040-7782 print/1521-0634 online
DOI: 10.1080/10407780802339064

Taylor & Francis
Taylor & Francis Group

NON-DARCIAN EFFECTS ON THE MIXED CONVECTION HEAT TRANSFER IN A METALLIC POROUS BLOCK WITH A CONFINED SLOT JET

Alia Marafie[1], Khalil Khanafer[2], Bader Al-Azmi[1], and Kambiz Vafai[3]

[1]*Mechanical Engineering Department, Kuwait University, Al-Safat, Kuwait*
[2]*Vascular Mechanics Laboratory, Department of Biomedical Engineering, University of Michigan, Ann Arbor, Michigan, USA*
[3]*Mechanical Engineering Department, University of California, Riverside, California, USA*

The present numerical investigation addresses non-Darcian effects on the mixed convection heat transfer in a metallic porous block with a confined slot jet. The generalized model of the momentum equation, which is also known as the Forchheimer-Brinkman extended Darcy model, was used in representing the fluid motion inside the porous layer. The local thermal equilibrium condition was assumed to be valid for the range of the thermophysical parameters considered in the present investigation. The transport equations were solved using the finite element formulation based on the Galerkin method of weighted residuals. The validity of the numerical code used was ascertained by comparing our results with previously published results. Our results revealed that the heat transfer performance of the slot jet was 2.4 times as large as that without the presence of a porous block. In addition, the average Nusselt number was found to increase with a decrease in porosity and an increase in the thermal conductivity ratio. The present results illustrate that the average Nusselt number increases with a decrease in the dimensionless height of the porous layer up to $H_{porous} = 0.05$, after which the Nusselt number decreases.

1. INTRODUCTION

Impinging jets have been used in many industrial applications to produce enhanced and controlled heating and cooling effects on surfaces. Such applications include turbine blade cooling, electronic components cooling, annealing of nonferrous sheet metals, tempering of glass and drying of textiles, wood, and paper [1]. Jet impingement has been studied extensively in the literature under various configurations [2–7]. Al-Sanea [1] developed a numerical model based on finite-volume approach for calculating the steady flow and heat-transfer characteristics of a laminar slot-jet impinging on an isothermal flat surface. The Nusselt number variation along the heat transfer surface showed an enhanced heat transfer rate around the

Received 2 May 2008; accepted 2 July 2008.
We acknowledge support for this work by the Kuwait University Research Grant No. ZE 03/08.
Address correspondence to Kambiz Vafai, Mechanical Engineering Department, University of California-Riverside, A363 Bourns Hall, Riverside, CA 92505, USA. E-mail: vafai@engr.ucr.edu

NOMENCLATURE

c_p	specific heat at constant pressure
Da	Darcy number, K/W_{jet}^2
F	Forchheimer constant
g	acceleration due to gravity
Gr	Grashof number, $g\beta\Delta T W_{\text{jet}}^3/\nu^2$
H	nondimensional height of the channel
H_{porous}	nondimensional height of porous block
J	unit vector oriented along the pore velocity vector
k	thermal conductivity
K	permeability of the porous medium
k_r	porous-to-fluid thermal conductivity ratio (k_s/k_f)
L_{porous}	length of the heated surface
L	nondimensional length of the heated surface, $L_{\text{porous}}/W_{\text{jet}}$
$\underline{\text{Nu}}$	local Nusselt number
$\overline{\text{Nu}}$	average Nusselt number
p	pressure
P	dimensionless pressure, $p/(\rho V_{jet}^2)$
Pr	Prandtl number, ν/α
Re	Reynolds number, $V_{\text{jet}} W_{\text{jet}}/\nu$
Ri	Richardson number, Gr/Re^2
t	time
T	temperature
T_C	temperature of the jet flow
T_H	temperature of the hot surface
$\mathbf{v}$	dimensional velocity vector
$\mathbf{V}$	dimensionless velocity vector, $\mathbf{v}/V_{\text{jet}}$
W_{jet}	width of the jet
x	x coordinate
(X, Y)	dimensionless coordinate, $(x,y)/W_{\text{jet}}$
y	y coordinate
α	thermal diffusivity
β	coefficient of thermal expansion
ε	porosity of the porous medium
λ	maximum-norm
ν	kinematic viscosity
θ	dimensionless temperature, $(T - T_C)/(T_H - T_C)$
$\theta_{\text{interface}}$	dimensionless temperature at the porous-fluid interface, $\frac{T(x,H_{\text{porous}})-T_C}{T_H-T_C}$
θ_{mid}	dimensionless temperature at the mid-section, $\frac{T(0,y)-T_C}{T_H-T_C}$
ρ	density
τ	dimensionless time, $tV_{\text{jet}}/W_{\text{jet}}$

Subscripts

eff	effective
f	fluid
porous	porous medium
s	solid

impingement region. Lee and Vafai [2] presented a comparative analysis of jet impingement and microchannel cooling for high heat flux applications. The authors concluded that the microchannel cooling was preferable for a target dimension smaller than 0.07 m by 0.07 m while the jet impingement was comparable or better than the microchannel cooling for a larger target plate if a proper treatment was applied for the spent flow after the impingement. Mikhail et al. [8] analyzed numerically flow and heat transfer characteristics of laminar jets issuing from a row of slots and impinging normally on a flat plate. Their results showed that the average Nusselt number increases with a decrease in the nozzle spacing. Using a similar approach, Yuan et al. [9] presented numerical predictions of the effects of buoyancy on a laminar slot-jet impinging on a flat surface. For high Richardson numbers, both buoyancy assisted and retarded flows were shown to have a significant effect on the enhancement and degradation, respectively, of the local Nusselt number.

Jet impingement cooling through porous medium has received relatively less attention in the literature. A study of the enhancement of the convection heat transfer of a laminar slot jet impinging on three different shape porous blocks (rectangle, convex, and concave) mounted on a heated region was investigated numerically by Fu and Huang [10]. Their results indicated that the heat transfer was mainly affected by a fluid flowing near the heated region. Jeng and Tzeng [11] studied numerically the air jet impingement cooling of a porous metallic foam heat sink in the forced

convection mode. Their results showed that the porous Aluminum foam heat sink enhances the heat transfer performance of an impinging jet. Same authors experimentally investigated convective heat transfer and pressure drop in the metallic porous block with a confined slot air jet [12] for various parameters such as the ratio of the jet nozzle width to the porous block height, the ratio of the jet-to-foam tip distance to the porous block height, and the jet Reynolds number. Their results indicated that the average Nusselt number increased with increased Reynolds number and decreased porous block height. Jet impingement cooling of a heated portion of a horizontal surface immersed in a fluid saturated porous media was investigated numerically by Saeid and Mohamad [13] based on using Darcy's law. It was found that the average Nusselt number increased with an increase in Rayleigh number and Péclet number. Recently, Saeid [14] studied numerically jet impingement cooling of heated portion of a horizontal surface immersed in a thermally nonequilibrium porous layer in the presence of a cross flow. The mathematical model was derived for steady, two-dimensional laminar flow based on a Darcy model and the use of the two-energy equation for fluid and solid phases. It was found that the presence of a weak cross flow in a jet impinging jet degraded the heat transfer. Moreover, the results showed the domination of the parallel flow and reduced the impact of the jet flow for high values of the cross flow to jet flow velocity ratio. Shih et al. [15] investigated experimentally heat transfer characteristics of aluminum-foam heat sinks with restricted flow outlets under impinging-jet flow conditions. The effects of porosity, pore density and length of the sample, air velocity, and flow outlet height on the heat transfer characteristics of aluminum-foam heat sinks were investigated. Results showed that the effect of the flow outlet height was stronger than that of the pore density, porosity, or height of the aluminum heat sinks studied in their work.

It is worth noting that the majority of the reviewed studies on jet impingement cooling of a horizontal surface in a confined porous medium were based on Darcy's law, which neglects the inertia and viscous effects on fluid flow and heat transfer. Since the rigid matrix resistance in a porous structure deviates from Darcy's law at high velocities, a generalized flow model (also known as the Brinkman-Forchheimer-extended Darcy model) was utilized in the present investigation to better analyze the transport processes in the presence of the coupling effect between the fluid-saturated porous medium and the fluid region. This work discusses how the height of the porous medium heat sink and the Richardson number influences the flow characteristics and the Nusselt number. Moreover, this investigation incorporates several pertinent dimensionless groups in conducting the analyses. These groups are the Richardson number, porous medium solid-to-fluid thermal conductivity ratio, Darcy number, the height of the porous block, porosity, and the height of the channel.

2. MATHEMATICAL FORMULATION

The problem under investigation is a two-dimensional steady flow and heat-transfer characteristics of a laminar slot-jet impinging on a metallic porous block mounted along the bottom surface of the channel. The physical domain under consideration and coordinate system are shown in Figure 1. The isothermal part of the impinging surface (over the length of the heat-transfer region, L_{porous}) is maintained

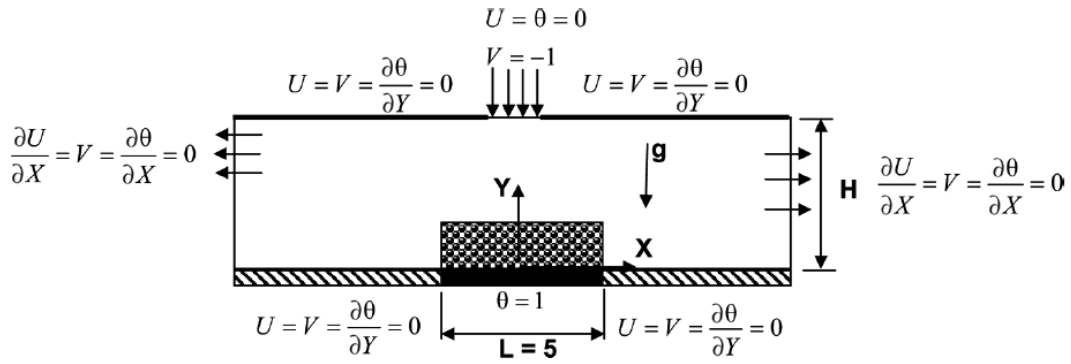

Figure 1. Schematic representation of the physical problem.

at a constant temperature T_H and the temperature of the fluid at the slot-jet exit is maintained at a constant temperature T_C. The porous medium is viewed as a continuum with the solid and fluid phases in thermal equilibrium, isotropic, homogeneous, and saturated with an incompressible Newtonian fluid. Furthermore, viscous heat dissipation in the fluid is assumed to be negligible in comparison to conduction and convection heat transfer effects. Also, it is assumed that the thermophysical properties of the fluid are independent of temperature except for the density in the buoyancy term, which is treated according to the Boussinesq approximation.

The governing equations in the porous domain are handled using the volume-averaging method. By incorporating the above points, the system of the governing equations can be expressed as [16–20]

Porous Layer

Continuity equation

$$\nabla \cdot < \boldsymbol{V} > = 0 \tag{1}$$

Momentum equation

$$\frac{1}{\varepsilon} < (\boldsymbol{V} \cdot \nabla)\boldsymbol{V} > = -\nabla < P >^{f} + \frac{1}{\varepsilon \mathrm{Re}} \nabla^2 < \boldsymbol{V} > - \frac{< \boldsymbol{V} >}{\mathrm{DaRe}} - \frac{\mathrm{F}\varepsilon}{\sqrt{\mathrm{Da}}} [< \boldsymbol{V} > \cdot < \boldsymbol{V} >] J + \frac{\mathrm{Gr}}{\mathrm{Re}^2} \theta \tag{2}$$

Energy equation

$$< \boldsymbol{V} > \cdot \nabla \theta = \frac{k_{\mathrm{eff}}}{k_f} \frac{1}{\mathrm{PrRe}} \nabla^2 \theta \tag{3}$$

where,

$$k_{\mathrm{eff}} = \varepsilon k_f + (1 - \varepsilon) k_s \tag{4}$$

The geometric function F in the momentum equation is given by

$$F = \frac{1.75}{\sqrt{150 \varepsilon^3}} \tag{5}$$

Fluid Layer

Continuity equation

$$\nabla \cdot \boldsymbol{V} = 0 \tag{6}$$

Momentum equation

$$\boldsymbol{V} \cdot \nabla \boldsymbol{V} = -\nabla P + \frac{1}{\mathrm{Re}} \nabla^2 \boldsymbol{V} + \frac{\mathrm{Gr}}{\mathrm{Re}^2} \theta \tag{7}$$

Energy equation

$$\boldsymbol{V} \cdot \nabla \theta = \frac{1}{\mathrm{PrRe}} \nabla^2 \theta \tag{8}$$

The above equations were normalized using the following dimensionless parameters.

$$\boldsymbol{V} = \frac{\mathbf{v}}{\boldsymbol{V}_{\mathrm{jet}}} P = \frac{p}{\rho \boldsymbol{V}_{\mathrm{jet}}^2} \theta = \frac{T - T_C}{T_H - T_C} x = \frac{(x, y)}{W_{\mathrm{jet}}} \tag{9}$$

where $\boldsymbol{V}_{\mathrm{jet}}$ is the jet velocity, W_{jet} is the jet width, ρ is the fluid density, g the gravitational acceleration, $J = \boldsymbol{V}/|\boldsymbol{V}|$ is a unit vector oriented along the pore velocity vector, P the dimensionless pressure, V the dimensionless velocity vector, and $\mathrm{Da} = K/W_{\mathrm{jet}}^2$ is the Darcy number. In addition, the relevant Grashof number, jet Reynolds number, and Prandtl number are given by $\mathrm{Gr} = g\beta\Delta T W_{\mathrm{jet}}^3/\nu^2$, $\mathrm{Re} = \boldsymbol{V}_{\mathrm{jet}} W_{\mathrm{jet}}/\nu$, and $\mathrm{Pr} = \nu/\alpha$, respectively. The flow and heat transfer characteristics are symmetrical around the y axis as shown in Figure 1. As such, the boundary conditions are

Inlet (jet exit plane)

$$U = \theta = 0 \quad \boldsymbol{V} = -1 \tag{10}$$

Outlet

The outlet boundary is located far enough downstream resulting in fully developed flow conditions. Accordingly, the following conditions are imposed at the exit.

$$\boldsymbol{V} = \frac{\partial U}{\partial X} = \frac{\partial \theta}{\partial X} = 0 \tag{11}$$

Walls

All walls are stationary and impervious and, hence, $U = \boldsymbol{V} = 0$. Normal gradients of temperature are set to zero at the adiabatic walls: $\partial\theta/\partial Y = 0$. For the isothermal part of the impinging surface, the temperature is set to $\theta = 1$.

The physical quantities of interest in the present investigation are the local and the average Nusselt numbers along the hot surface which are defined respectively as

$$\left(\mathrm{Nu} = -\frac{\partial \theta}{\partial Y}\right)_{Y=0} \Rightarrow \overline{\mathrm{Nu}} = \frac{1}{L} \int_0^L \mathrm{Nu}\, dX \tag{12}$$

where L is the nondimensional length of the isothermal surface (heated surface of the porous block, as shown in Figure 1).

3. NUMERICAL SCHEME

A finite element formulation based on the Galerkin method was employed to solve the governing equations. The application of this technique is well documented by Taylor and Hood [21] and Gresho et al. [22]. In the current investigation, the continuum domain was divided into a set of nonoverlapping regions called elements. Nine node quadrilateral elements with bi-quadratic interpolation functions were utilized to discretize the physical domain. Moreover, interpolation functions in terms of local normalized element coordinates were implemented to approximate the dependent variables within each element. Subsequently, substitution of the approximations into the system of the governing equations and boundary conditions yielded a residual for each of the conservation equations. These residuals were then reduced to zero in a weighted sense over each element using the Galerkin method.

The highly coupled and nonlinear algebraic equations resulting from the discretization of the governing equations were solved using a segregated-solution algorithm. The advantage of this method is that the global system matrix is decomposed into smaller submatrices and then solved in a sequential manner. This technique resulted in considerably fewer storage requirements. A pressure projection algorithm was utilized to obtain a solution for the velocity field at every iteration step. Furthermore, the pressure projection version of the segregated algorithm was used to solve the nonlinear system. In addition, the conjugate residual scheme was used to solve the symmetric pressure-type equation systems, while the conjugate gradient squared method was used for the nonsymmetric advection-diffusion-type equations.

4. GRID REFINEMENT

Many numerical experiments of various mesh sizes were performed to attain grid-independent results and to determine the best compromise between accuracy and minimizing computer execution time. As such, a variable grid-size system was employed in the present investigation to capture the rapid changes in the dependent variables especially near the solid boundaries and the fluid-porous interface where the major gradients occur inside the boundary layer. The solution was assumed to have converged when the relative variation of the average Nusselt number between two consecutive iterations was less than 0.01%. As an additional check on the convergence to a steady-state solution, the standard relative error based on the maximum-norm (λ) was used:

$$\lambda = \frac{\| \boldsymbol{V}^{n+1} - \boldsymbol{V}^{n} \|_{\infty}}{\| \boldsymbol{V}^{n+1} \|_{\infty}} + \frac{\| \theta^{n+1} - \theta^{n} \|_{\infty}}{\| \theta^{n+1} \|_{\infty}} \leq 10^{-6} \tag{13}$$

where the operator $\| \ \|_{\infty}$ indicates the maximum absolute value of the variable over all grid points in the computational domain.

Table 1 Comparison of the average Nusselt number in a cavity filled with a porous medium between the present results and that of Nithiarasu et al. [23] and Chen et al. [24] for various Rayleigh numbers ($\varepsilon = 0.9$, $Da = 10^{-2}$)

Ra	Nu [present]	Nu [23]	Nu [24]
1×10^3	**1.02**	1.023	1.02
1×10^4	**1.63**	1.63	1.63
1×10^5	**3.93**	3.91	3.92
5×10^5	**6.69**	6.70	NA

5. VALIDATION

The present numerical code was validated against the numerical results of Nithiarasu et al. [23] and Chen et al. [24] for the average Nusselt number in a cavity filled with a porous medium between using the generalized momentum equation. Table 1 displays comparison for the average Nusselt number between the present results and the numerical results of Nithiarasu et al. [23] and Chen et al. [24]. As an additional check on the accuracy of the present code, the average Nusselt number for the present study was validated against the numerical results of Al-Sanea [1] for a laminar slot-jet impinging on an isothermal flat surface, as shown in Figure 2, for various jet-Reynolds numbers. Both Table 1 and Figure 2 display very good agreement between the current results and the prior works.

6. RESULTS AND DISCUSSION

The results presented in this work were obtained for different pertinent dimensionless groups: Richardson number ($0.01 \leq \mathrm{Ri} \leq 1$), Darcy number ($10^{-2} \leq \mathrm{Da} \leq 10^{-6}$), channel height ($0.5 \leq H \leq 4$), height of the porous layer ($0.005 \leq$

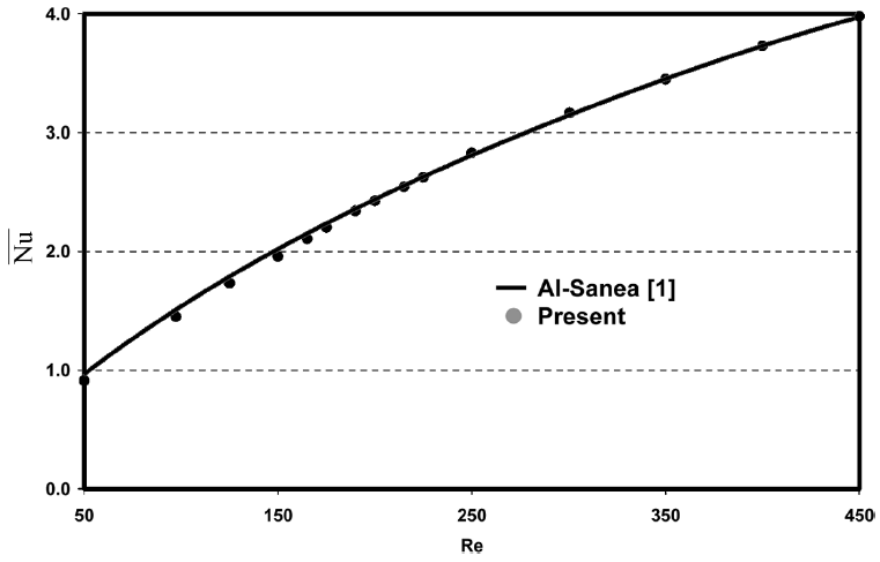

Figure 2. Comparison of the average Nusselt number between present results and that of Al-Sanea [1] for a laminar slot-jet impinging on an isothermal flat surface.

$H_{\text{porous}} \leq 3$), porosity of the porous layer ($0.25 \leq \varepsilon < 1$), and thermal conductivity ratio ($1 \leq k_s/k_f \leq 200$). The default parameters were assigned values of $H = 4$, $H_{\text{porous}} = 0.25$, $\text{Ri} = 0.01$, $k_s/k_f = 5$, $\varepsilon = 0.93$, $\text{Da} = 10^{-2}$, $\text{Pr} = 1$, $\text{L} = 5$, and $\text{Re} = 100$ unless otherwise stated. The predicted field variables were presented in terms of the streamlines, isotherms, interface temperature and average Nusselt number.

6.1. Effect of the Porous Medium Solid-to-Fluid Thermal Conductivity Ratio (k_s/k_f)

The effect of varying the porous medium solid-to-fluid thermal conductivity on streamlines and isotherms is presented in Figure 3. It is apparent in Figure. 3 that as the conductivity ratio increases, the porous medium becomes more conductive and the strength of the convective flow in the porous layer decreases leaving the porous layer almost isothermal for high thermal conductivity ratio. Further, Figure 3

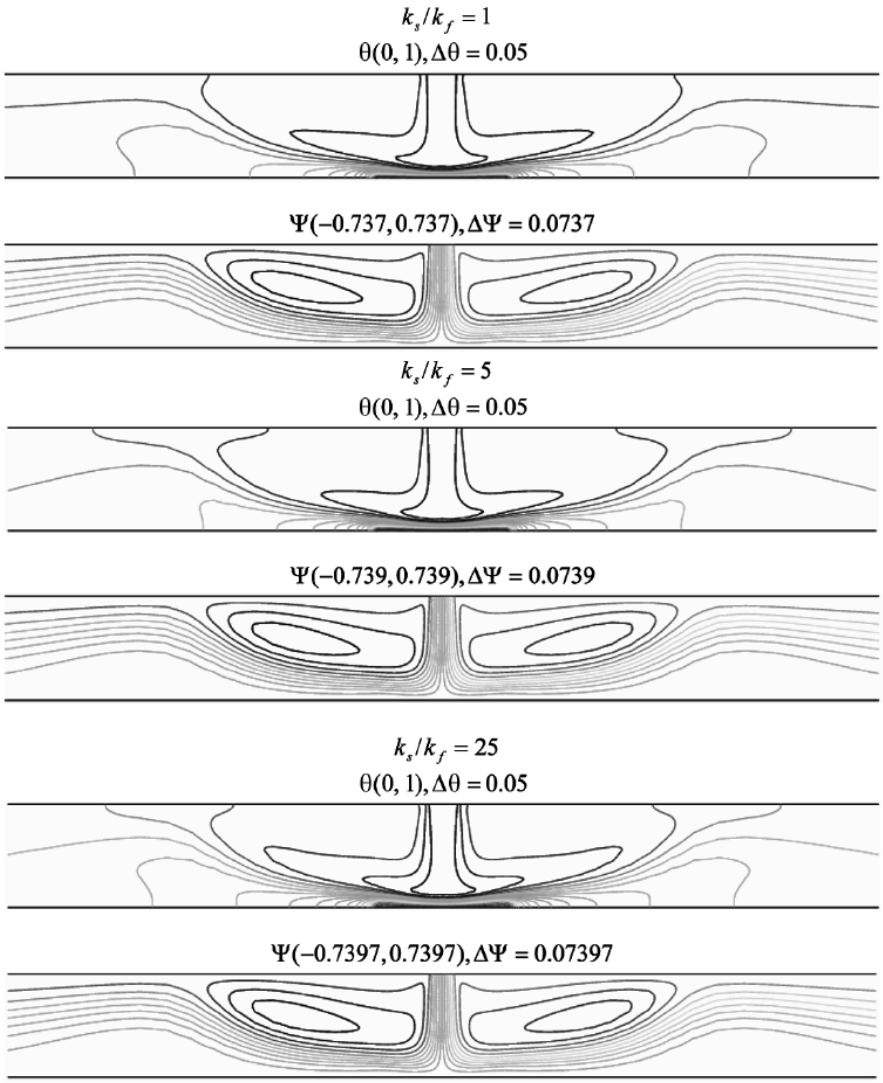

Figure 3. Effect of k_s/k_f on the streamlines and isotherms ($\text{Re} = 100$, $\text{Ri} = 0.01$, $H_{\text{porous}} = 0.25$, $H = 4$, $\varepsilon = 0.93$, and $\text{Da} = 10^{-2}$).

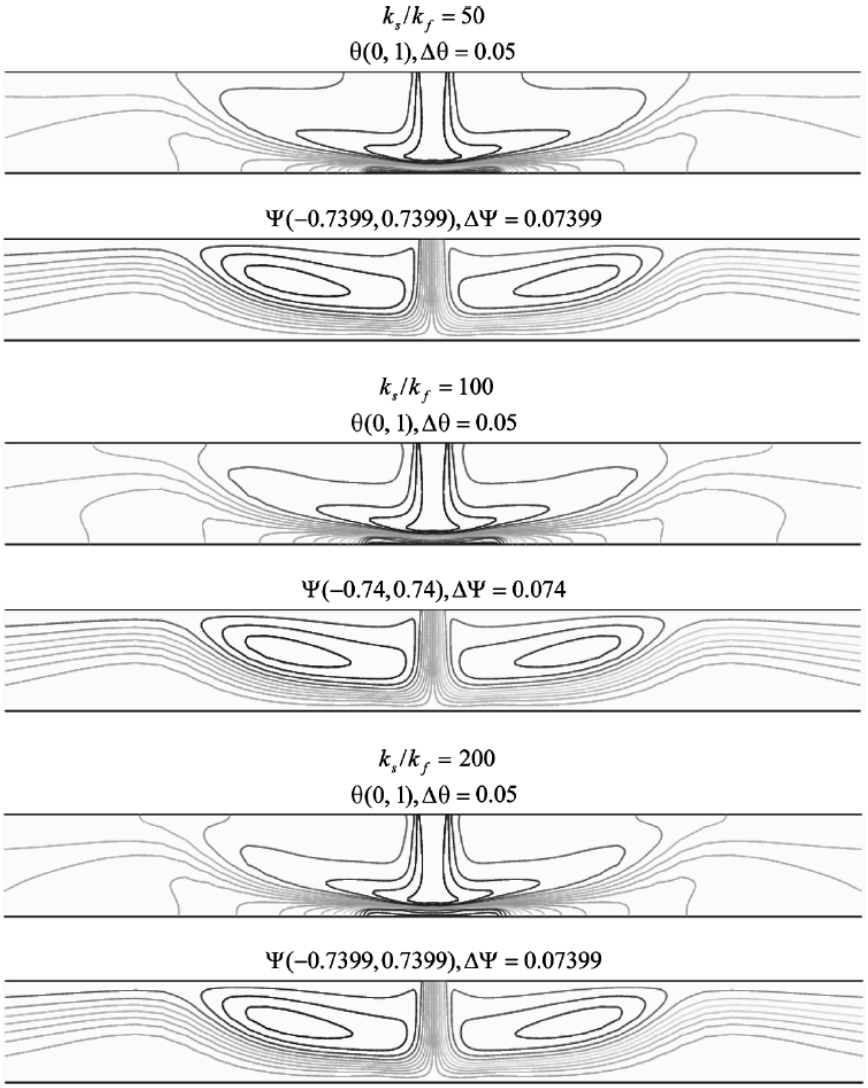

Figure 3. Continued.

illustrates that the conductivity ratio (k_s/k_f) has an insignificant effect on the streamlines. However, this effect is more pronounced for the temperature and the Nusselt number distributions, as shown in Figures 4–6. Figures 4–6 illustrate the implications of varying k_s/k_f on the average Nusselt number, interface temperature, and mid-section temperature. Figure 4 shows that the overall heat transfer rate is enhanced with an increase in the thermal conductivity ratio due to large temperature gradients offered in the fluid layer. As such, the average Nusselt number increases rapidly for $k_s/k_f < 25$ as depicted from large slope of the average predicted Nusselt number. Thereafter, for $k_s/k_f < 25$, the average Nusselt number increases at a lower rate as indicated by the slope of the average Nusselt number. The influence of thermal conductivity ratio (k_s/k_f) on the interface temperature between the porous and fluid layers is shown in Figure. 5. This figure demonstrates that the porous layer is almost isothermal for large k_s/k_f (i.e., $k_s/k_f = 200$). It is worth noting that the lowest temperature value occurs at the center of the top surface of

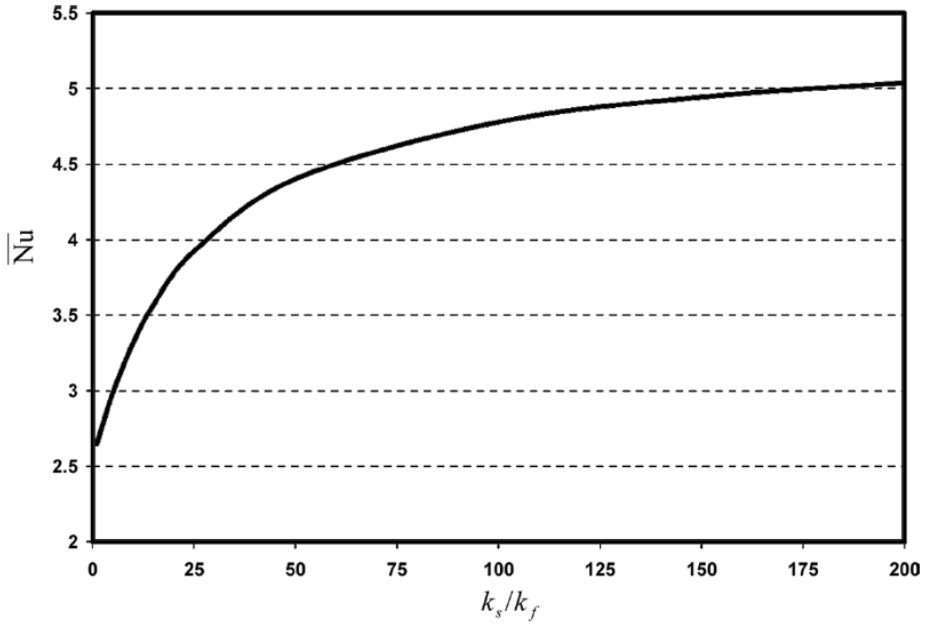

Figure 4. Effect of k_s/k_f on the average Nusselt number (Re = 100, Ri = 0.01, $H_{\text{porous}} = 0.25$, $H = 4$, $\varepsilon = 0.93$, and $\text{Da} = 10^{-2}$).

the porous layer. This is associated with the effect of the low temperature impinging jet flow on the top surface of the porous layer. Similarly, Figure. 6 illustrates the impact of the thermal conductivity ratio on the temperature profiles along a vertical plane passing through the middle of the porous medium. This figure confirms that the porous layer is almost isothermal for large k_s/k_f since the temperature difference across the porous block for $k_s/k_f = 200$ is much smaller than for the case of low k_s/k_f.

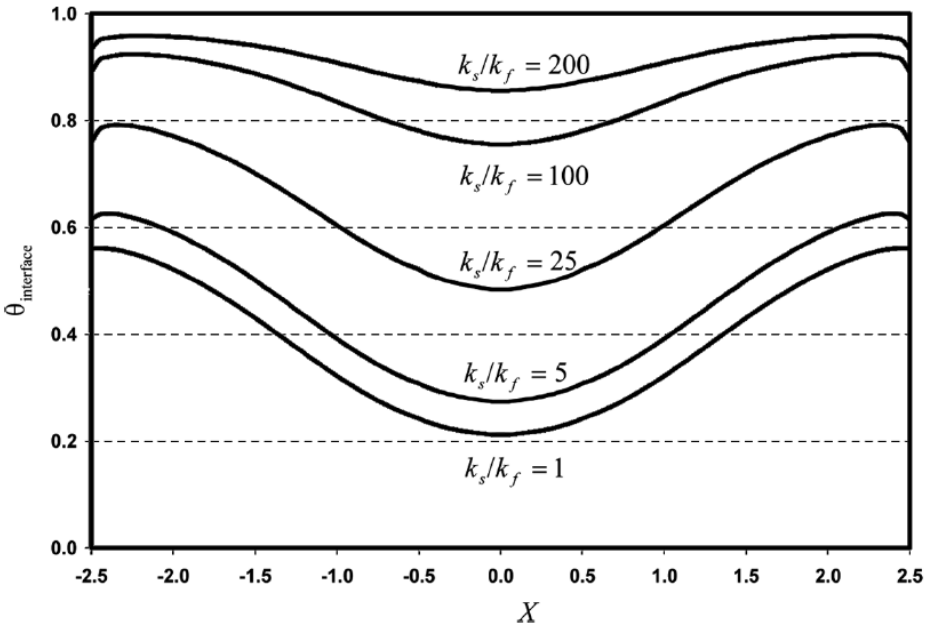

Figure 5. Effect of k_s/k_f on the temperature profiles along the interface between the porous medium and the fluid domain (Re = 100, Ri = 0.01, $H_{\text{porous}} = 0.25$, $H = 4$, $\varepsilon = 0.93$, and $\text{Da} = 10^{-2}$).

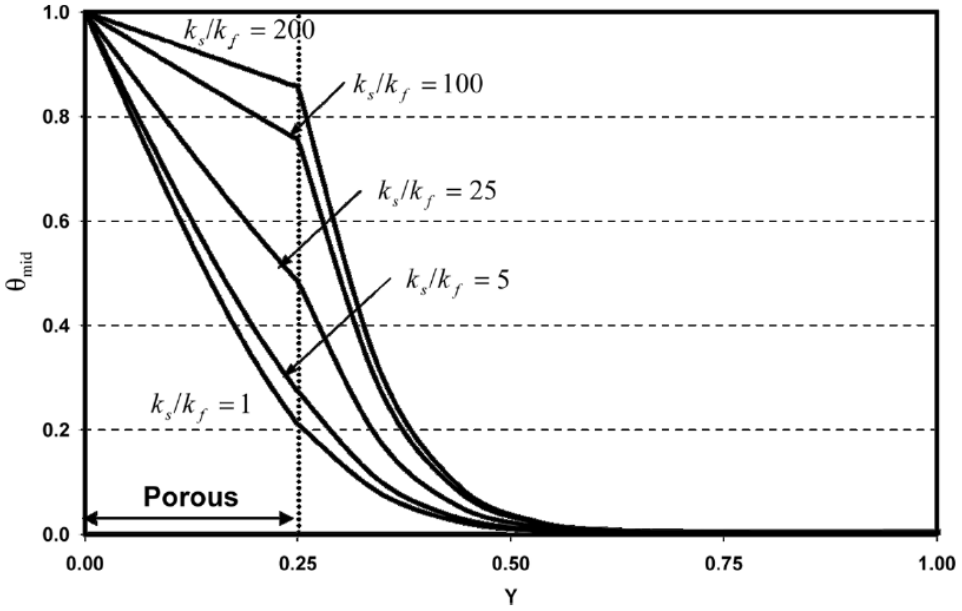

Figure 6. Effect of k_s/k_f on the temperature profiles along a vertical plane passing through the middle of the porous medium (Re = 100, Ri = 0.01, $H_{\text{porous}} = 0.25$, $H = 4$, $\varepsilon = 0.93$, and Da = 10^{-2}).

6.2. Effect of Porous Medium Height

The effect of changing the height of the porous layer on the streamlines and isotherms is depicted in Figure 7. This figure shows that as the height of the porous block (i.e., heat sink) increases, the intensity of the streamlines decreases due to high flow resistance offered by the porous block which causes a significant reduction in the size of the recirculation zone above the porous layer. Figure 8 shows the impact of increasing the height of the porous layer on the average Nusselt number for various Reynolds number. This figure demonstrates that the average Nusselt number increases with the decrease of the dimensionless height of the porous layer until $H_{\text{porous}} = 0.05$, and then the Nusselt number decreases. The increase in the Nusselt number results from the decreased flow resistance as the height of the porous layer decreases, whereas the decrease in the average Nusselt number is caused by an increase in the flow resistance as the height of the porous layer increases. Figure 8 reveals that the average Nusselt number with the metallic porous block was 2.4 times as large as that without the porous layer. The effect of the porous layer height on the interface temperature between the fluid and porous layers is illustrated in Figure 9. The top surface of the porous layer is almost at a uniform temperature corresponding to the jet flow temperature for larger height.

6.3. Effect of Channel Height

Streamline plots and isotherms are used to illustrate the nature of the flow and temperature fields and their dependence on the channel height, as depicted in Figure 10. The minimum and maximum values of the stream functions and isotherms are written on the top of each figure. Twenty equal intervals are used to

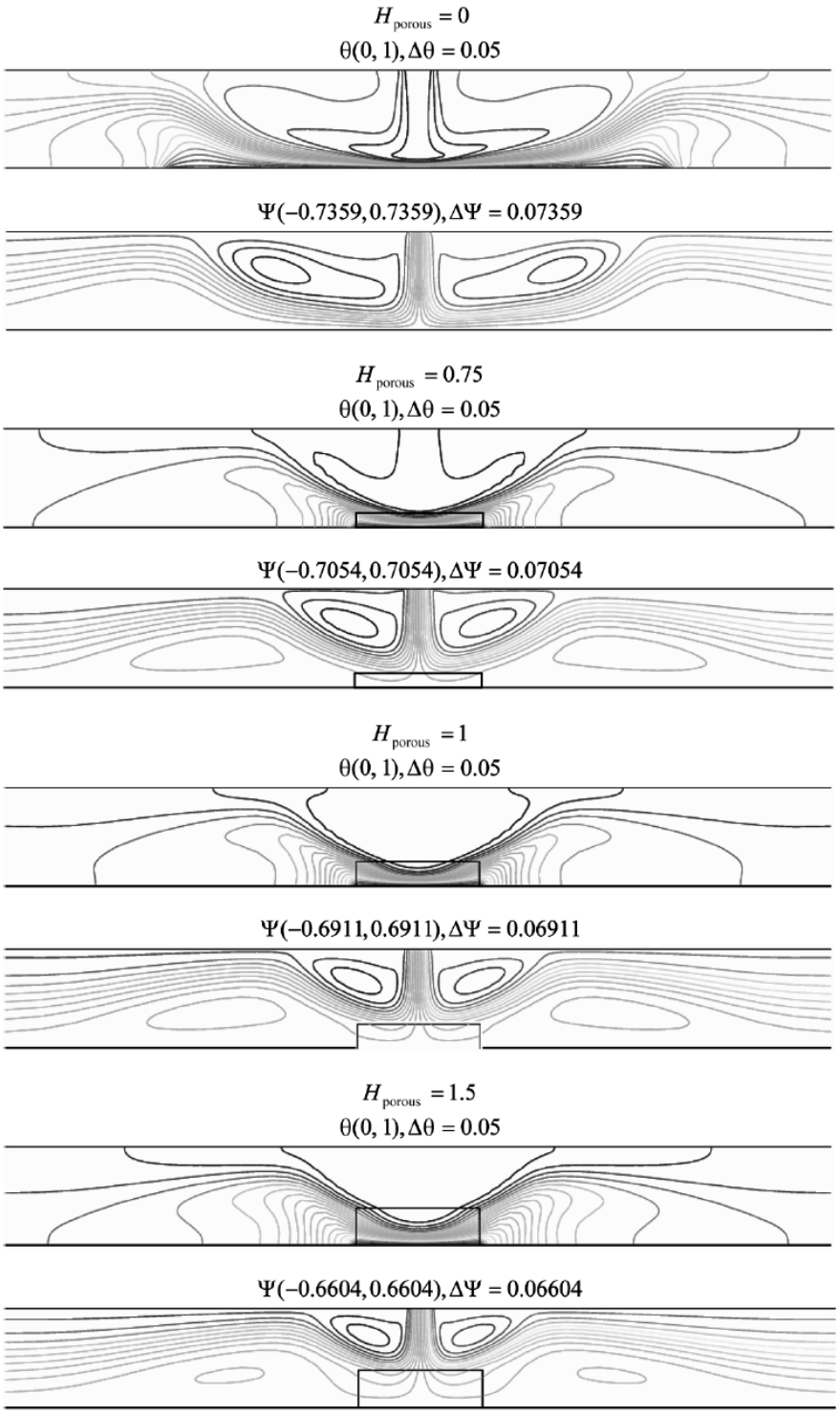

Figure 7. Effect of the porous medium height on the streamlines and isotherms (Re = 100, Ri = 0.01, $H = 4$, $\varepsilon = 0.93$, $k_s/k_f = 5$, and Da = 10^{-2}).

represent the streamlines and isotherms. Positive values of streamlines correspond to counterclockwise flow and negative values characterize clockwise flow. It can be noticed in Figure 10 that the circulation cells between the impinging jet and the confining wall disappear for a small normalized channel height ($H < 1$). As the

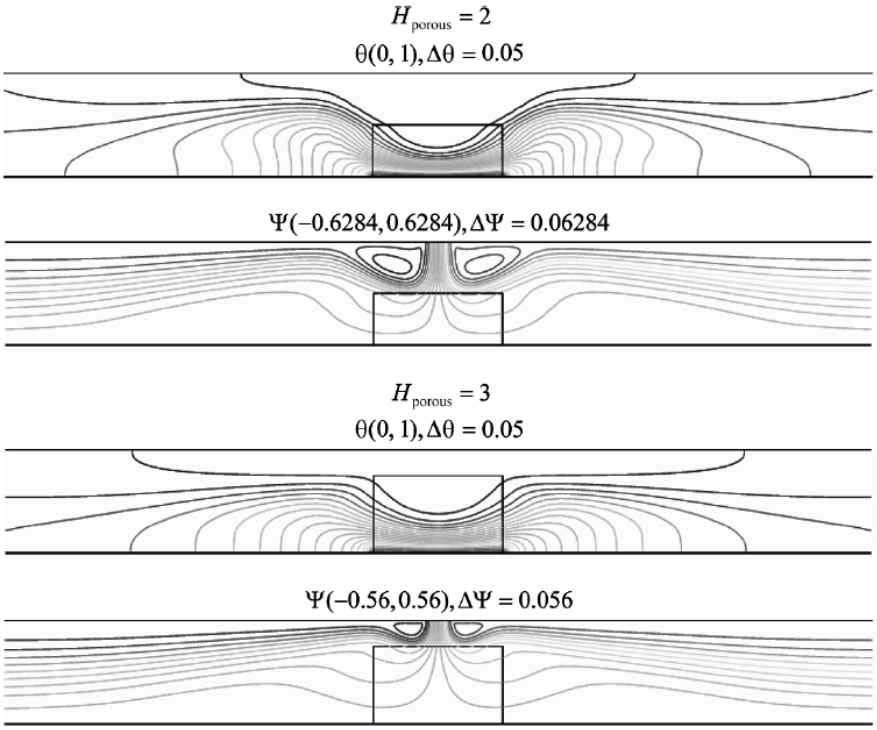

Figure 7. Continued.

normalized channel height increases, the circulation cell in the fluid layer increases in size and strength, as depicted in Figure 10. This trend is due to the fact that downstream of the nozzle, as the height of the channel increases, the shear layer progressively grows and displaces the potential core. The effect of the channel height

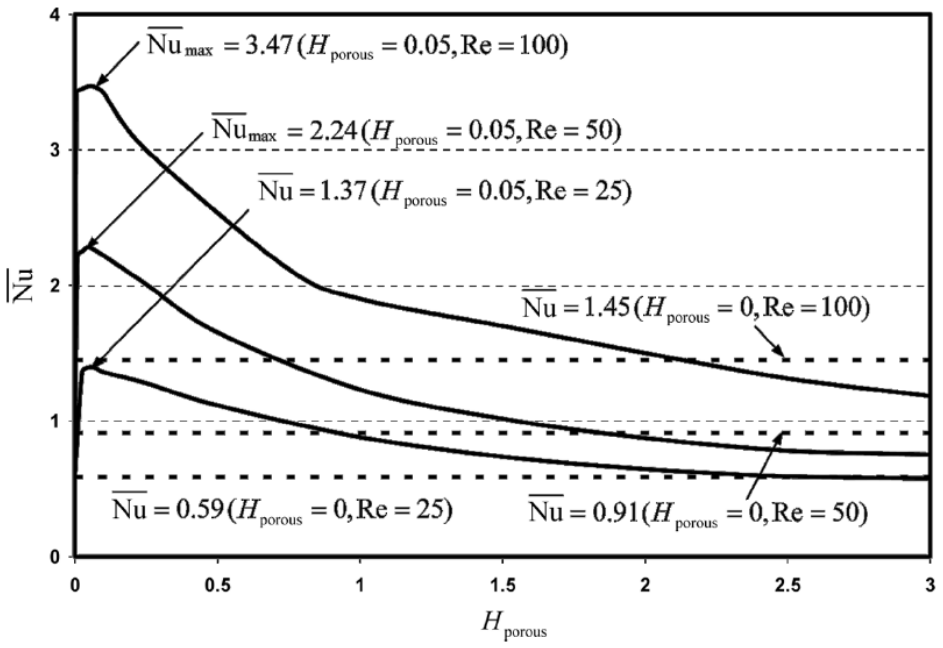

Figure 8. Effect of the porous medium height on the average Nusselt number for various Reynolds numbers (Ri = 0.01, $k_s/k_f = 5$, $H = 4$, $\varepsilon = 0.93$, and Da = 10^{-2}).

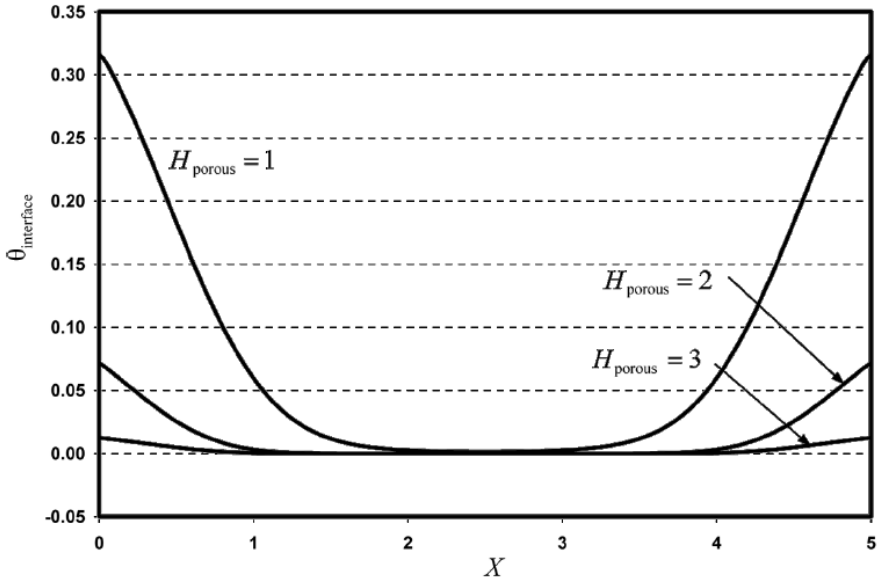

Figure 9. Effect of the porous medium height on the temperature profiles along the interface between the porous medium and the fluid domain (Re = 100, Ri = 0.01, $k_s/k_f = 5$, $H = 4$, $\varepsilon = 0.93$, and Da = 10^{-2}).

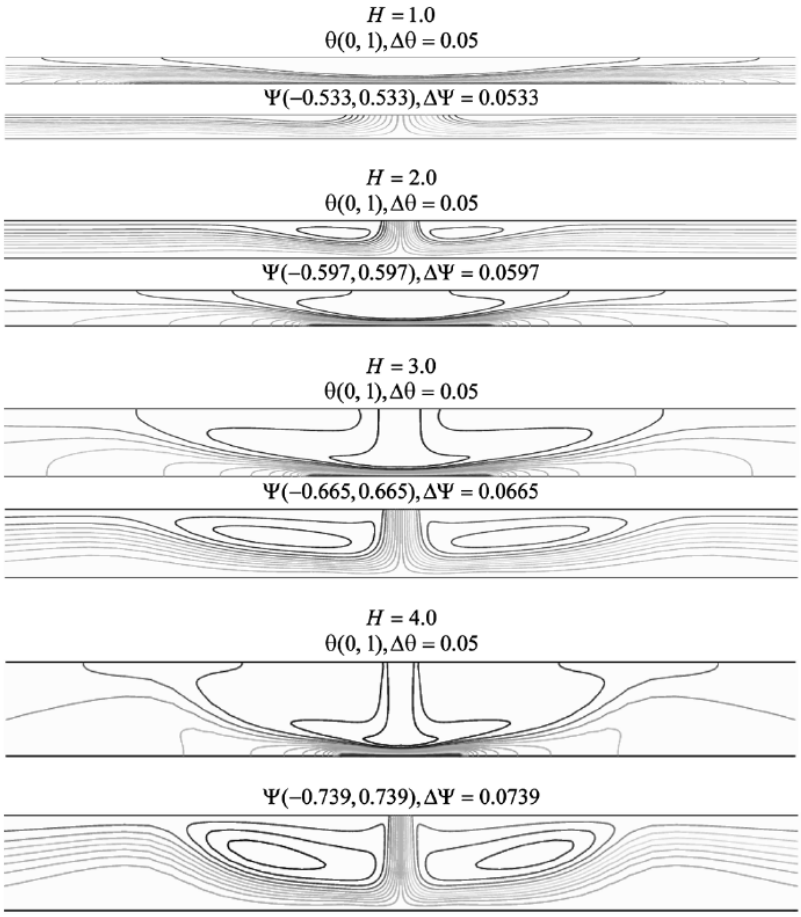

Figure 10. Effect of the channel height on the streamlines and isotherms (Re = 100, Ri = 0.01, $H_{\text{porous}} = 0.25$, $\varepsilon = 0.93$, $k_s/k_f = 5$, and Da = 10^{-2}).

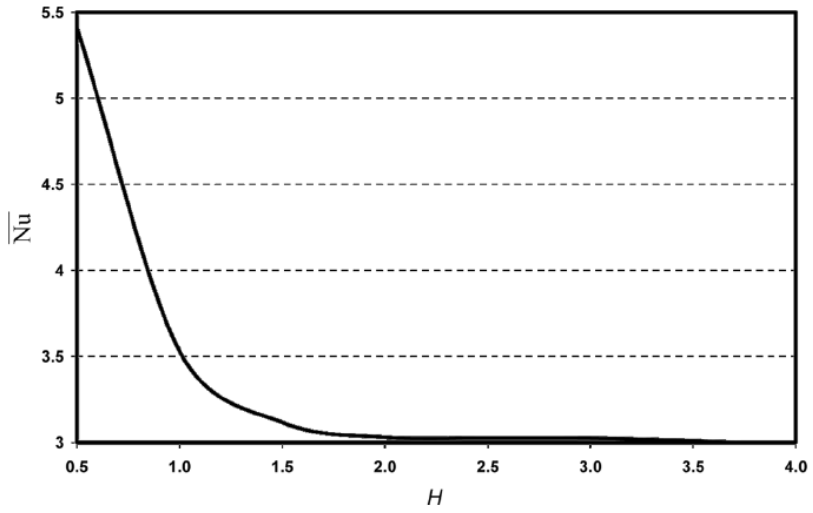

Figure 11. Effect of the channel height on the average Nusselt number ($\mathrm{Re} = 100,\ \mathrm{Ri} = 0.01,\ k_s/k_f = 5,$ $H_{\mathrm{porous}} = 0.25, \varepsilon = 0.93,$ and $\mathrm{Da} = 10^{-2}$).

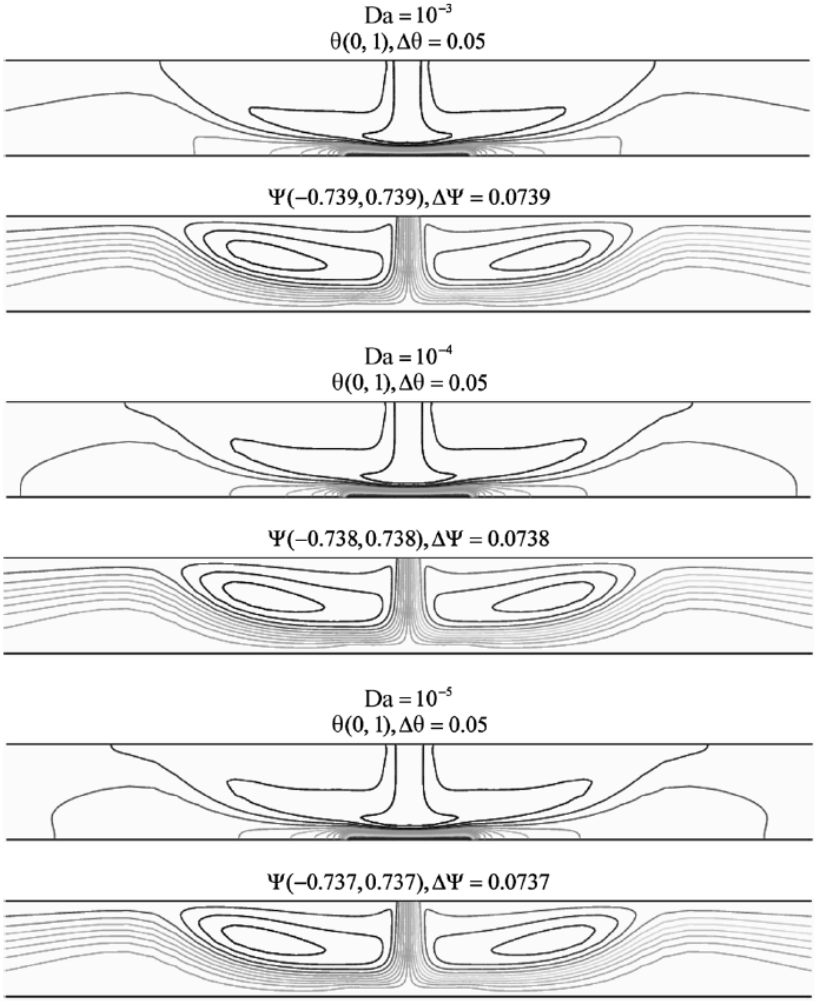

Figure 12. Effect of the Darcy number on the streamlines and isotherms ($\mathrm{Re} = 100,\ \mathrm{Ri} = 0.01,$ $H_{\mathrm{porous}} = 0.25,\ H = 4,\ \varepsilon = 0.93,$ and $k_s/k_f = 5$).

on the average Nusselt number is shown in Figure 11. It can be noticed in Figure 11 that the average Nusselt number decreases with an increase in the channel height because the interface temperature between the porous layer and the fluid layer increases.

6.4. Effect of Darcy Number and Porosity

The effect of the Darcy number on the streamlines and isotherms is illustrated in Figure 12. As can be seen, the Darcy number has an insignificant effect on the intensity of flow activities as well as the isotherms within the fluid layer for small Richardson numbers (Ri = 0.01). The Richardson number provides a measure for the importance of the thermal natural convection forces relative to the forced convection. For a small Richardson number, the buoyancy effect is overwhelmed by the effect of jet flow. The effect of the Darcy number on the average Nusselt number is illustrated in Figure 13. For small values of Darcy numbers, the porous layer is considered less permeable to fluid penetration and consequently the fluid experiences a pronounced large resistance as it flows through the porous matrix. This results in hindering flow activities in the porous region and consequently decreases the average Nusselt number, as depicted in Figure 13, and increases the interface temperature between the fluid layer and porous layer as, illustrated in Figure 14. The effect of the porosity on the average Nusselt number and the temperature profiles along the interface between the porous and fluid layers are shown in Figures 15 and 16. As the porosity of the porous medium decreases, the average Nusselt number increases as depicted in Figure 15. This is associated with an increase in the effective thermal conductivity of porous medium. Therefore, the temperature along the interface of the porous and fluid layers decreases with an increase in the porosity, as depicted in Figure 16.

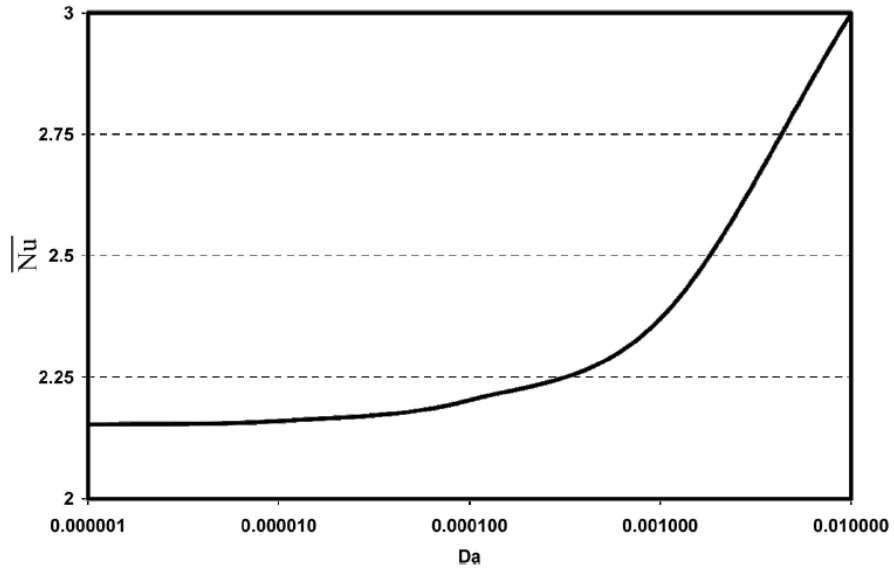

Figure 13. Effect of the Darcy number on the average Nusselt number (Re = 100, Ri = 0.01, $k_s/k_f = 5$, $H_{\text{porous}} = 0.25$, $H = 4$, and $\varepsilon = 0.93$).

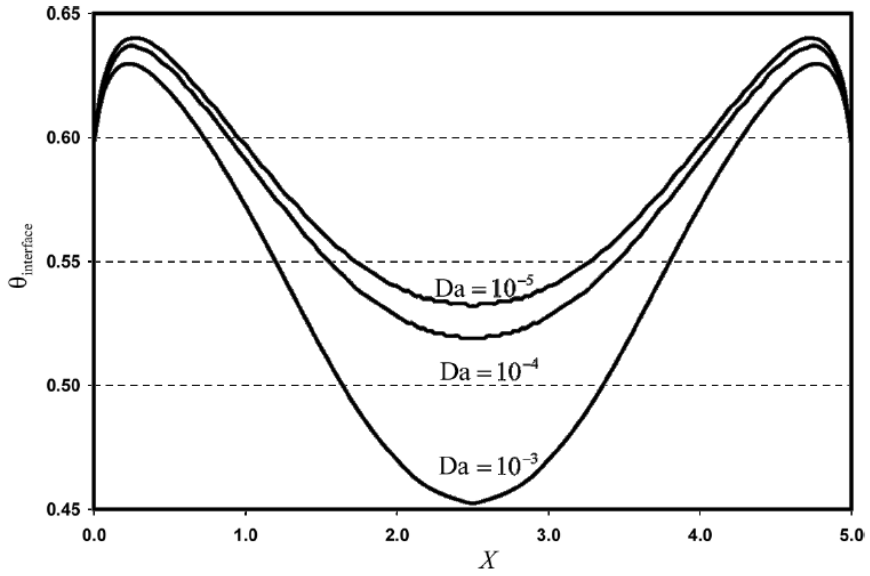

Figure 14. Effect of the Darcy number on the temperature profiles along the interface between the porous medium and the fluid domain (Re = 100, Ri = 0.01, $k_s/k_f = 5$, $H_{\text{porous}} = 0.25$, $H = 4$, and $\varepsilon = 0.93$).

6.5. Effect of Richardson Number

The total heat transfer rate between the jet flow and the heated surface is related to the average heat transfer coefficient, which is best represented by the average Nusselt number. Figure 17 depicts the effect of the Richardson number on the average Nusselt number. It is observed in Figure 17 that increasing the Richardson number (or increasing the Grashof number) increases the average Nusselt number.

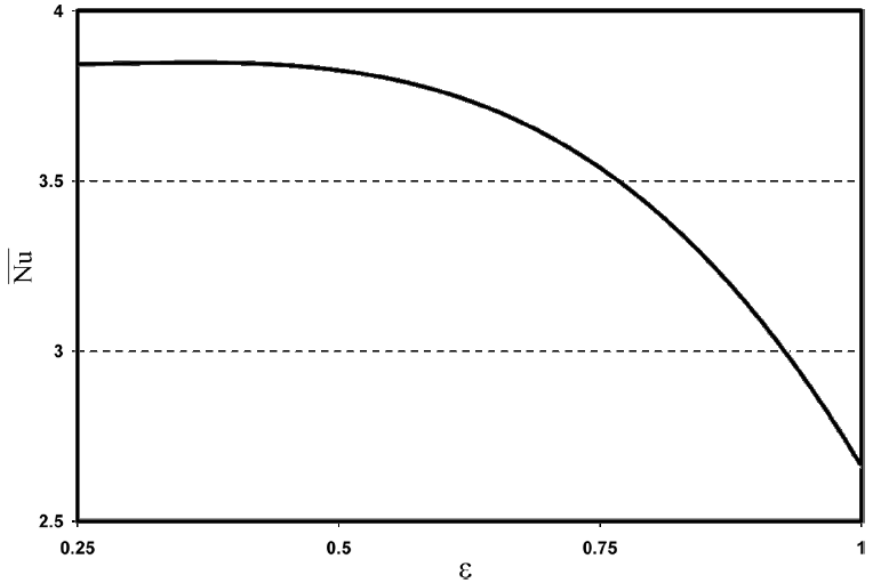

Figure 15. Effect of the porosity on the average Nusselt number (Re = 100, Ri = 0.01, $k_s/k_f = 5$, $H_{\text{porous}} = 0.25$, $H = 4$, and Da = 10^{-2}).

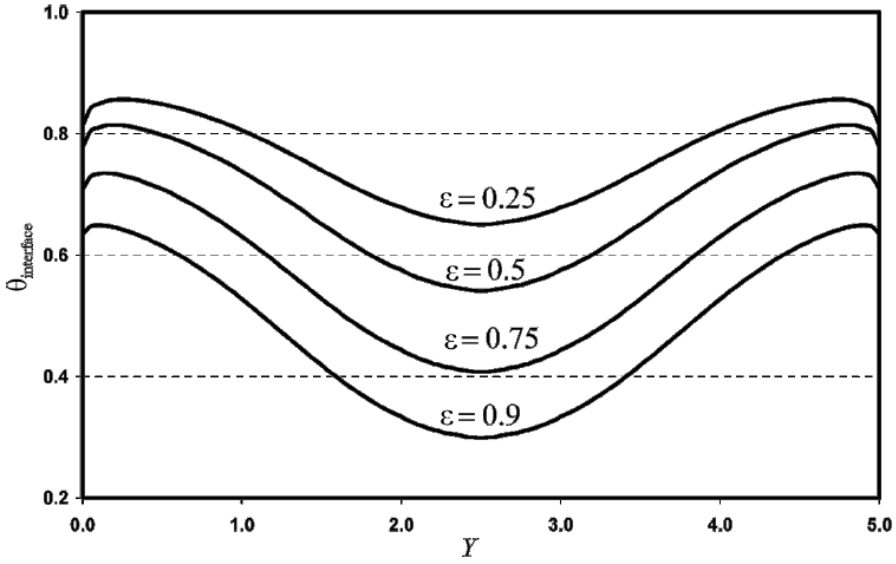

Figure 16. Effect of the porosity on the temperature profiles along the interface between the porous medium and the fluid domain (Re = 100, Ri = 0.01, $k_s/k_f = 5$, $H_{\text{porous}} = 0.25$, $H = 4$, and Da = 10^{-2}).

This is due to the fact that as the Grashof number increases convection heat transfer within the porous layer becomes more pronounced.

6.6. Heat Transfer Correlation

The average Nusselt number calculated along the bottom heated porous layer is correlated in terms of various pertinent parameters including the Richardson

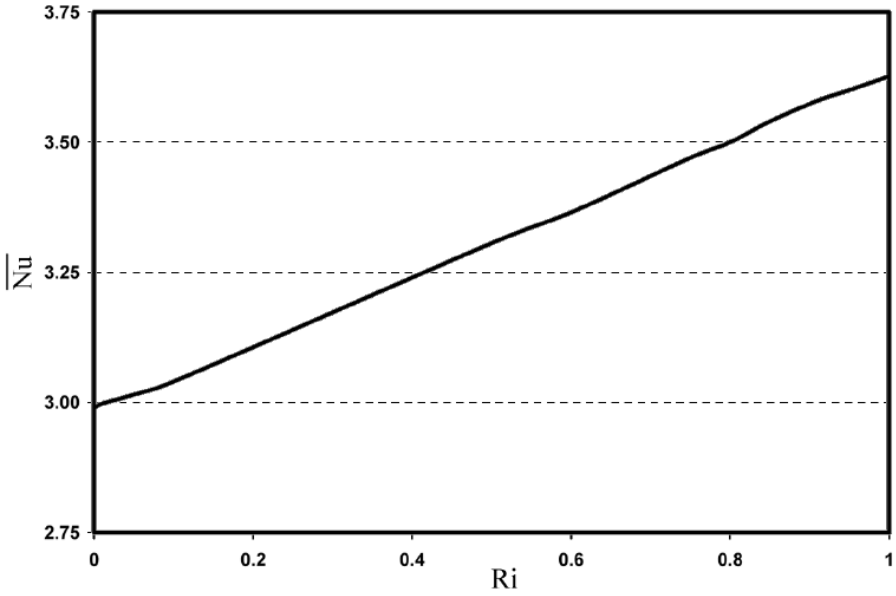

Figure 17. Effect of the Richardson number on the average Nusselt number (Re = 100, $k_s/k_f = 5$, $H_{\text{porous}} = 0.25$, $H = 4$, and Da = 10^{-2}).

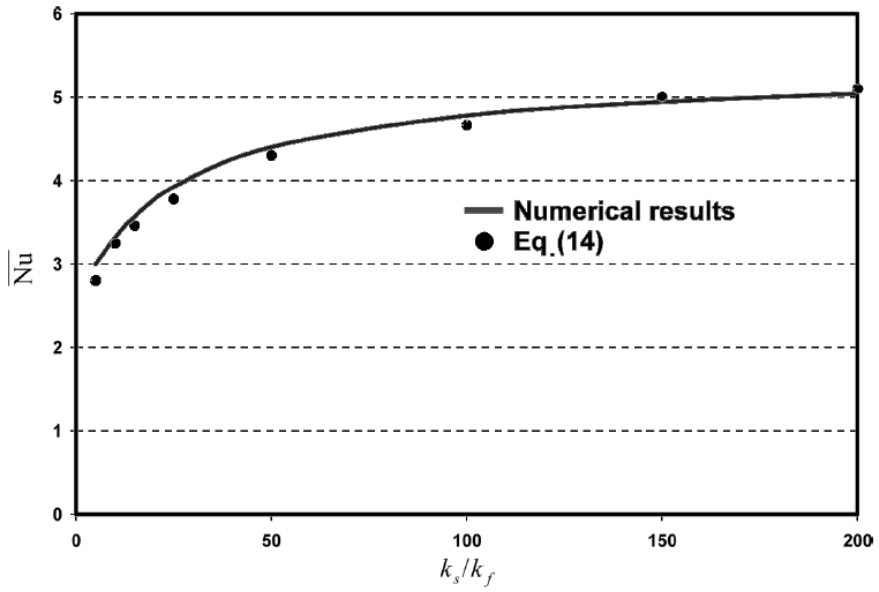

Figure 18. Comparison of the average Nusselt number between the present numerical results and Eq. (14) for various thermal conductivity ratio ($\varepsilon = 0.93$, $Re = 100$, $Ri = 0.01$, $H_{porous} = 0.25$, $H = 4$, and $Da = 10^{-2}$).

number ($0.01 \leq Ri \leq 1$), Darcy number ($10^{-2} \leq Da \leq 10^{-6}$), channel height ($0.5 \leq H \leq 4$), height of the porous layer ($0.005 \leq H_{porous} \leq 3$), and thermal conductivity ratio ($1 \leq k_s/k_f \leq 200$) The porosity of the porous layer was kept constant ($\varepsilon = 0.93$). This correlation can be written as follows.

$$\overline{Nu} = 9.4975 Ri^{0.0468} (k_s/k_f)^{0.17} Da^{0.0452} H^{-0.2639} (1.7915 + H_{porous})^{-0.9873} \qquad (14)$$

where the confidence coefficient for the above equation is $R^2 = 93\%$. A graphical representation of the above correlation is shown in Figure 18. This figure demonstrates an excellent agreement between the numerical results and those obtained by the correlation.

7. CONCLUSIONS

Non-Darcian effects on mixed convection heat transfer in a metallic porous block with a confined slot jet were studied numerically for various pertinent dimensionless groups. Effects of dimensionless groups representing the Richardson number, Darcy number, heights of the channel and porous layer, porosity, and thermal conductivity ratio were highlighted to study their impacts on flow structure and heat transfer characteristics. The results reveal that there is a substantial increase in heat removal capability using a porous block. Narrowing the distance between the jet and the heated portion and decreasing the porosity of the porous medium could also increase the average Nusselt number. Moreover, the higher solid-to-fluid thermal conductivity ratio of the porous medium is found to significantly improve the average Nusselt number. Finally, a Nusselt number correlation was established for a wide range of the considered dimensionless groups in this investigation.

REFERENCES

1. S. Al-Sanea, A Numerical Study of the Flow and Heat Transfer Characteristics of an Impinging Laminar Slot-Jet Including Cross-Flow Effects, *Int. J. Heat Mass Transfer*, vol. 35, pp. 2501–2513, 1992.
2. D.Y. Lee and K. Vafai, Comparative Analysis of Jet Impingement and Microchannel Cooling for High Heat Flux Applications, *Int. J. Heat Mass Transfer*, vol. 31, pp. 1555–1568, 1999.
3. F. J. Higuera and M. Martinez, An Incompressible Jet in a Weak Crossflow, *J. Fluid Mech.*, vol 249, pp. 73–97, 1993.
4. A. J. Humber, E. W. Grandmaison, and A. Pollard, Mixing Between a Sharp-Edged Rectangular Jet and a Transverse Cross Flow, *Int. J. Heat Mass Transfer*, vol. 36, pp. 4307–4316, 1993.
5. L. B. Y. Aldabbagh, I. Sezai, and A. A. Mohamad, Three-Dimensional Investigation of a Laminar Impinging Square Jet Interaction with Cross-Flow, *ASME J. Heat Transfer*, vol. 125, pp. 243–249, 2003.
6. D. H. Lee, J. Song, and M. C. Jo, The Effects of Nozzle Diameter on Impinging Jet Heat Transfer and Fluid Flow, *ASME J. Heat Transfer*, vol. 126, pp. 554–557, 2004.
7. X. Li, J. L. Gaddis, and T. Wang, Multiple Flow Patterns and Heat Transfer in Confined Jet Impingement, *Int. J. Heat Fluid Flow*, vol. 26, pp. 746–754, 2005.
8. S. Mikhail, S. M. Morcos, M. M. M. Abou-Ellail, and W. S. Ghaly, Numerical Prediction of Fow Field and Heat Transfer from a Row of Laminar Slot Jets Impinging on a Flat Plate, *Proc. 7th Znt. Heat Transfer Conf.*, vol. 3, pp. 377–382, 1982.
9. T. D. Yuan, J. A. Liburdy, and T. Wang, Buoyancy Effects on Laminar Impinging Jets, *Int. J. Heat Mass Transfer*, vol. 31, pp. 2137–2145, 1988.
10. W. S. Fu and H. C. Huang, Thermal Performance of Different Shape Porous Blocks Under an Impinging Jet, *Int. J. Heat Mass Transfer*, vol. 40, pp. 2261–2272, 1997.
11. T. M. Jeng and S. C. Tzeng, Numerical Study of Confined Slot Jet Impinging on Porous Metallic Foam Heat Sink, *Int. J. Heat Mass Transfer*, vol. 48, pp. 4685–4694, 2005.
12. T. M. Jeng and S. C. Tzeng, Experimental Study of Forced Convection in Metallic Porous Block Subject to a Confined Slot Jet, *Int. J. Thermal Sciences,* vol. 46, pp. 73–89, 2007.
13. N. H. Saeid and A. A. Mohamad, Jet Impingement Cooling of a Horizontal Surface in a Confined Porous Medium: Mixed Convection Regime, *Int. J. Heat Mass Transfer*, vol. 49, pp. 3906–3913, 2006.
14. N. H. Saeid, Jet Impingement Interaction with Cross Flow in Horizontal Porous Layer Under Thermal Non-Equilibrium Conditions, *Int. J. Heat Mass Transfer*, vol. 50, pp. 4265–4274, 2007.
15. W. H. Shih, F. C. Chou, and W. H. Hsieh, Experimental Investigation of the Heat Transfer Characteristics of Aluminum-Foam Heat Sinks with Restricted Flow Outlet, *J. Heat Transfer*, vol. 129, pp. 1554–1563, 2007.
16. K. Khanafer and K. Vafai, The Role of Porous Media in Biomedical Engineering as Related to Magnetic Resonance Imaging and Drug Delivery, *Heat and Mass Transfer*, vol. 42, pp. 939–953, 2006.
17. A. Amiri and K. Vafai, Analysis of Dispersion Effects and Nonthermal Equilibrium, Non-Darcian, Variable Porosity Incompressible-Flow Through Porous-Media, *Int. J. Heat Mass Transfer*, vol. 37, pp. 939–954, 1994.
18. A. Amiri and K. Vafai, Transient Analysis of Incompressible Flow Through a Packed Bed, *Int. J. Heat Mass Transfer*, vol. 41, pp. 4259–4279, 1998.
19. K. Vafai and C. L. Tien, Boundary and Inertia Effects on Convective Mass Transfer in Porous Media, *Int. J. Heat and Mass Transfer*, vol. 25, pp. 1183–1190, 1981.

20. K. Vafai and C L. Tien, Boundary and Inertia Effects on Flow and Heat Transfer in Porous Media, *Int. J. Heat and Mass Transfer*, vol. 24, pp. 195–203, 1980.
21. C. Taylor and P. Hood, A Numerical Solution of the Navier-Stokes Equations using Finite-Element Technique, *Comput. Fluids*, vol. 1, pp. 73–89, 1973.
22. P. M. Gresho, R. L. Lee, and R. L. Sani, On the Time-Dependent Solution of the Incompressible Navier-Stokes Equations in Two and Three Dimensions, In *Recent Adv. Num. Methods in Fluids*, Pineridge, Swansea, UK, vol. 1, pp. 27–79, 1980.
23. P. Nithiarasu, K. N. Seetharanu, and T. Sundararajan, Natural Convective Heat Transfer in a Fluid Saturated Variable Porosity Medium, *Int. J. Heat Mass Transfer*, vol. 40, pp. 3955–3967, 1997.
24. X. B. Chen, P. Yu, S. H. Winoto, and H. T. Low, Free Convection in a Porous Cavity based on the Darcy-Brinkman-Forchheimer Extended Model, *Numerical Heat Transfer A*, vol. 52, pp. 377–397, 2007.